Astron. Astrophys. 340, 163–177 (1998)

ASTRONOMY
AND
ASTROPHYSICS

Multi-line analysis of the spectra of Herbig Ae/Be stars⋆

J.-C. Bouret[1] **and C. Catala**[1]

Laboratoire d'Astrophysique de Toulouse, CNRS UMR 5572, Observatoire Midi-Pyrénées, 14, avenue Edouard Belin, F-31400 Toulouse, France

Received 1 July 1998 / Accepted 22 September 1998

Abstract. We present the results of the study of four Herbig Ae/Be stars (AB Aur, BD+46°3471, HD250550, BD+61°154). For each of them, semi-empirical models of the structure of their winds have been constructed; we then calculated the $H\alpha$ line, the Balmer discontinuity, as well as the C IV 1548 Å and Mg II h or k resonance lines. Thanks to comparison with observational data, we have deduced constraints on the parameters of the models, which provide us with a rather good representation of the averaged structure of the winds. Despite of the time variability of these stars, we show that we can gather trustworthy information on the values of the mass loss rates of these stars. It is also shown that models with departure from spherical symmetry are needed to account for the observed shapes of the lines. In addition, radiative losses due to several transitions (lines and continua) of hydrogen have been evaluated, in order to gain more insight in the energy sources that generate the observed activity of these stars.

Key words: stars: atmospheres – stars: individual: AB Aur – stars: individual: BD+46°3471 – stars: individual: BD+61°154 – stars: individual: HD 250550 – stars: pre-main sequence

1. Introduction

One of the major problems raised by the Herbig Ae/Be stars is the strong activity they exhibit. Indeed, most of them present spectral signatures of the presence of heated layers in their outer atmosphere, such as emission lines, lines of highly ionized species, X-ray emission (Catala et al. 1986a, Hamman & Person 1992, Zinnecker & Preibisch 1994; Bouret et al. 1997). Furthermore, PCygni profiles of Mg II h and k and of hydrogen Balmer lines are often observed, these profile being characteristic of stellar winds. These winds and activity phenomena remain unexplained in the Herbig Ae/Be stars.

Convection is unlikely to play a decisive role, since according to the theory of stellar evolution (Iben 1965, Gilliland 1986, Palla & Stahler 1993), pre-main sequence stars with intermediate masses (2-5$M_{\odot}$) and spectral types A or B, possess at the best very thin outer convection zones.

One commonly invoked explanation for the wind and active phenomena of the Herbig Ae/Be stars is linked to a circumstellar accretion disk (Corcoran & Ray, 1998). Such a disk may indeed drive a radiative wind with adequate mass loss rates and terminal velocities, as suggested by Proga et al. (1998) and Drew et al. (1998). Moreover, the release of the disk gravitational energy in a boundary layer at the stellar surface may be the source of the observed active phenomena; this mechanism was first proposed to explain the Balmer excess of classical T Tauri stars (Bertout et al. 1988, Kenyon & Hartmann 1987).

However, the presence of accretion disks around the Herbig Ae/Be stars is controversial. The disk model invoked by Hillenbrand et al. (1992) to account for the infrared excesses of the Herbig Ae/Be stars has been criticized by Berrilli et al. (1992) and Hartmann et al. (1993), who explain the observed IR excesses with spherical dust envelopes. More recently Pezzuto et al. (1997) showed that the spectral energy distribution of a large group of Herbig Ae/Be stars is well explained by a spherically symmetric model for matter distribution, the dust being constituted by noncrystalline particles. Böhm & Catala (1993), then Ghandour et al. (1994) found no significant optical veiling on the spectra of a sample of Herbig Ae/Be stars, while circumstellar disks with the accretion rates derived from the model of Hillenbrand et al. (1992) would inevitably produce one. Finally, Böhm & Catala (1994) and Corcoran & Ray (1997) observed that those Herbig Ae/Be stars that are less deeply embedded in their parental cloud exhibit symmetric and unshifted forbidden [O I] lines, in contrast to the majority of classical T Tauri stars or the deeply embedded Herbig Ae/Be stars, which show strongly asymmetric and blueshifted forbidden lines. Such asymmetries and blueshifts are interpreted as evidence for an optically thick accretion disk that hides the receding half of a wind in which the forbidden lines are formed (Appenzeller et al. 1983, Appenzeller et al. 1984). The conclusion is thus that at least a large fraction of the Herbig Ae/Be stars, including many stars with strong winds and active phenomena, do not possess such ac-

Send offprint requests to: J.-C. Bouret (bouret@obs-mip.fr)

⋆ Based on observations with the Bernard Lyot 2m telescope at Pic du Midi Observatory, France, the archives of the International Ultraviolet Explorer (IUE) collected at the Villafranca Satellite Tracking Station of the European Space Agency, and the archives of the Hubble Space Telescope, collected at the Space Telescope Science Institute in Baltimore.

cretion disks, and therefore that the source of their winds and activity must be looked for elsewhere.

Deuterium burning in a subsurface shell may entertain a convection zone, which itself may produce a dynamo-generated magnetic field responsible for the observed active phenomena (Palla & Stahler, 1990,1991,1992,1993). However, since deuterium burning occurs on a much shorter timescale than the pre-main sequence timescale at these masses, it is necessary to invoke continuous accretion of fresh deuterium at a very high rate to account for the observation of active phenomena in the majority of the Herbig Ae/Be stars. Because of the poor observational evidence for accretion disks in these stars, this model thus suffers from the same difficulties as the disk wind and boundary layer activity models.

Finally, a model has been proposed by Vigneron et al. (1990), then revisited by Tout & Pringle (1995), and completed recently by Lignières et al. (1996), in which rotational braking of the star via a strong stellar wind excites turbulent motions below the star's surface. These turbulent motions would be responsible for a dynamo that generates the magnetic field needed to sustain activity.

Whatever the ultimate source of energy responsible for the winds and activity of the Herbig Ae/Be stars, there is growing evidence that magnetic fields play an important role in controlling these phenomena. First of all, rotational modulation of lines formed in the wind of several Herbig Ae/Be stars was reported (Praderie et al. 1986, Catala et al. 1986b, Catala et al. 1989, Catala et al. 1991, Beskrovnaya et al. 1995, Böhm et al. 1996). This modulation is interpreted in terms of corotating streams controlled by a surface magnetic field. Second, Donati et al. (1997) have recently reported the direct detection of a surface magnetic field in the southern Herbig Ae star HD 104237.

It has been suggested that the corotating streams responsible for the rotational modulation also give rise to corotating interaction regions (CIRs), similar to those of the solar wind (Catala et al. 1986b); in that case, they could also explain the X-ray emission that has been reported by Zinnecker & Preibisch (1994) from ROSAT observations. The X-ray flux would be produced in the CIRs, resulting from shocks between fast and slow streams, these shocks heating the gas up to temperatures of several million degrees.

Clearly a better knowledge of the wind structure of a sample of Herbig Ae/Be stars is needed to constrain the mechanisms responsible for driving the wind and heating the chromosphere. In particular, reliable estimates of the mass loss rates, of the radiative losses, as well as constraints on the velocity law and on the detailed structure of the chromospheric regions would provide quantitative tests for the theoretical models of these stars. Such is the goal of the present paper.

Most of the lines that are clues for activity (e.g. Si IV, C IV, He I 5876 Å) present similar shapes in many Herbig Ae/Be stars, which suggests that similarities exist in the structure of their winds. In particular, for all stars belonging to the PCygni subclass, i.e. displaying a P Cygni profile at Hα (Finkenzeller & Mundt, 1984), the model proposed by Catala & Kunasz (1987) for AB Aur's wind, seems to be very promising. This semi-empirical model includes mass loss, a deep extended chromosphere and a cooler outer region, both expanding. In this paper, we extend the same type of models to three other stars of the P Cygni subclass.

Sect. 2, is devoted to the description of the selection of the stars sample, and to a brief presentation of the observational material available, including a discussion of the line variability. In Sect. 3 we present the atmospheric model we have used, the atomic model and the method of solution of the transfer equation. Sect. 4 deals with the analysis of the influence of each parameter of the model and Sect. 5 presents the results of the study for each one of the four stars. In Sect. 6 we discuss some properties of the model for these stars. Finally a general conclusion is given in Sect. 7.

2. Observational background

2.1. Selection of the star sample

The stars for this analysis were selected according to two major criteria: (i) presence of a P Cygni profile at $H\alpha$, and (ii) measured Balmer discontinuity.

The first criterion ensures that the star is losing mass through a stellar wind; the other types of $H\alpha$ profiles exhibited by the Herbig Ae/Be stars (single- and double-peaked emission) are ambiguous and may indicate other types of circumstellar environment and therefore are not suited to the analysis presented here. In addition, Catala et al. (1986a) have shown that Herbig stars with a P Cygni profile at $H\alpha$ have similar profiles in other lines probing various regions of their winds. The structures of these winds are therefore basically similar, and may be represented by a single class of models.

The second criterion is based on a previous study of the wind of AB Aur by Catala & Kunasz (1987), which showed that the Balmer discontinuity in Herbig Ae/Be stars is very sensitive to the temperature and electron density at the base of the wind, and therefore provides very powerful constraints on the wind structure when used in conjonction with $H\alpha$ and other line profiles.

Only six stars meet these criteria: AB Aur, BD+46°3471, HD250550, BD+61°154, Z CMa, and MWC 1080. Of these, Z CMa is now known to be a binary system in which the optical component is a FU Orionis star (Koresko et al. 1991, Leinert et al. 1997), while MWC 1080 is also a binary system (Shevchenko et al. 1994), with controversial spectral types for the two components (Cohen & Kuhi 1979, Yoshida et al. 1991). Our models are not suitable for such configurations, and we therefore removed these stars from our sample. The basic stellar parameters for the four remaining stars are listed in Table 1, together with the measured Balmer discontinuities (Garrison, 1978).

In addition to $H\alpha$ and Balmer discontinuity, we introduced in this analysis the modelling of the Mg II h & k and C IV resonance lines, when available. These UV lines are sensitive to the location, size and temperature of the chromosphere at the base of the wind, as demonstrated in the case of AB Aur by Catala et al. (1984), and Catala (1988).

Table 1. Stellar parameters and Balmer discontinuities. (1) Hillenbrand et al. 1992, (2) Garrison 1978, (3) Böhm & Catala 1993

Star	Sp. Type	log T_{eff}	$R_\star$ ($R_\odot$)	log(g)	D_B
AB Aur	A0 (3)	4.0 (3)	2.5 (3)	4.1 (3)	+1.4±0.05 (2)
BD+46°3471	A0 (1)	3.99 (1)	11.3 (1)	4.5 (2)	+1.08±0.08 (2)
HD250550	B7 (1)	4.09 (1)	3.5 (1)	4.6 (2)	+1.00±0.05 (2)
BD+61°154	B8 (1)	4.05 (1)	4.8 (1)	4.2 (2)	+0.29±0.08 (2)

2.2. Observational material

2.2.1. The $H\alpha$ line

For BD+61°154 and HD250550 we used $H\alpha$ line profiles obtained in 1991 with the MUSICOS spectrograph (Baudrand & Böhm 1992) at the Telescope Bernard Lyot (2m), at the Pic du Midi observatory. As regards AB Aur, we constructed an averaged $H\alpha$ profile by summing spectra recorded during the 1996 MUSICOS campaign (Catala et al. 1998). Concerning the reduction of the spectra, the reader is refered to Böhm & Catala (1993) for more details. We used for BD+46°3471 a profile recorded in 1983 at CFHT (see Catala et al. 1986a).

For comparison between the observed spectra and the synthetic one, each spectrum was adjusted to the frame of the interstellar Na I D lines, assumed to be identical to the star's rest frame (Böhm & Catala, 1993; Finkenzeller & Jankovics, 1984).

2.2.2. The Mg II h and k UV lines

IUE long wavelength spectra of AB Aur were recorded in 1992 before the MUSICOS campaign of the same year, while for HD250550 and BD+46°3471, IUE long wave observations were obtained in January 1984 and January 1983 respectively. We used the Mg II resonance lines of these three stars in our analysis, which all exhibit a P Cygni profile. The continuum was placed interactively in two line-free spectral regions (2758 Å and 2844 Å). The interstellar Mg I λ 2852.13 Å, appearing on the spectra, was used as reference for the wavelength scale.

2.2.3. The C IV 1548 Å line

For the C IV resonance doublet of AB Aur, we used observations with GHRS aboard the Hubble Space Telescope, obtained in 1996 (Bouret et al. 1997). HD250550 was observed with IUE in 1985. The continuum used for normalization was placed by hand, using the same procedure as that used by Catala & Talavera (1984). Because of the presence of many broad lines around the C IV resonance doublet (not seen on IUE spectra because of the lower resolution, but clearly visible on GHRS spectrum of AB Aur), this normalization is uncertain, possibly affecting the comparison with the synthetic profiles. The C IV resonance lines of both AB Aur and HD250550 are purely in absorption.

No high resolution UV spectra are available for BD+61°154.

Table 2 summarizes all the observational data at our disposal.

2.3. Variability

Repeated observations have shown that the lines used in this analysis are variable in Herbig Ae/Be stars. The absorption component of the $H\alpha$ PCygni profile of AB Aur, BD+46°3471 and HD 250550 is highly variable on time scales from hours to months (Böhm et al. 1996, Beskrovnaya et al. 1995), and sometimes even disappears to leave the $H\alpha$ line as a single emission (Shevchenko 1991, Beskrovnaya et al. 1991, 1995, Pogodin 1992, 1994,). The emission component of $H\alpha$ is also variable on similar time scales, although at a much lower level (Böhm et al. 1996, Catala et al. 1998, in preparation). Comparisons of $H\alpha$ line profiles of AB Aur obtained at different dates indicate that variations of the emission intensity are much less important than those of the absorption component (Catala & Kunasz 1987).

The absorption component of the Mg II resonance lines in the same three stars is always present, but shows strong variability both in its width and depth, modulated with the star's rotation in the case of AB Aur (Praderie et al. 1986). At the same time, the Mg II emission component shows intensity variations of the order of only 12%.

The C IV resonance lines of AB Aur, always in absorption, also exhibit important width and depth variations (Catala & Talavera 1984; Catala et al. 1986a; Bouret et al. 1997).

This variable behavior indicates a complex wind structure. In particular, the rotational modulation of the absorption component of the Mg II lines of AB Aur (Praderie et al. 1986), and possibly that of the C IV resonance lines (Catala et al. 1986a) was interpreted in terms of co-rotating azimuthal structures in the wind. Other models, like those of Pogodin (1990, 1992), involve a variable latitudinal dependence of the wind structure, and can explain the drastic changes observed in the $H\alpha$ absorption component. It is therefore very likely that the winds of the Herbig Ae/Be stars are neither spherically symmetric nor stationary, and their modelling by our time-independent, spherically symmetric models is only intended to bring information on the wind average properties.

The emission components of the $H\alpha$ and Mg II P Cygni profiles seem to vary much less than the absorption components. Catala et al. (1984) and Catala & Kunasz (1987) have shown that they are formed in very extended regions of the wind, and therefore can provide average information of the wind structure. On the other hand, absorption components of P Cygni profiles are formed in the parts of the winds that are projected on the stellar surface from the observer's point of view, and encompass only a small volume. Absorption components are therefore expected to be very sensitive to local variations in density, temperature and velocity on the line of sight to the observer, while emission components are more likely to represent average wind properties. We have therefore restricted the following analysis to the detailed interpretation of the $H\alpha$ and Mg II emission components, assuming that the absorption components of these lines cannot provide useful information in the framework of our stationary, spherically symmetric model. We have also made sure that our model can reproduce the presence in absorption of the

Table 2. Summary of observational data:(1) Averaged profile from the MUSICOS 1996 campaign. (2) GHRS/HST spectrum (Bouret et al. 1997). (3) Profile from IUE, recorded for the MUSICOS 1992 campaign. (4) Profiles from MUSICOS at TBL/Pic du Midi (Böhm & Catala 1994). (5) Profiles from IUE archives. (6) CFHT profile from Catala et al. (1986a)

star	AB Aur		HD250550		BD+46°3471		BD+61°154	
	Date	Instr.	Date	Instr.	Date	Instr.	Date	Instr.
$H\alpha$	Nov. 96	MUS. (1)	Oct. 91	MUS (4)	Sep. 83	CFHT (6)	Oct. 91	MUS (4)
C IV	Feb. 96	GHRS (2)	Jan. 85	IUE (5) SWP 24984	–	–	–	–
Mg II	Oct. 92 LWP 24207	IUE (3)	Jan. 84	IUE (5) LWP 2663	Jan. 83	IUE (5) LWP 1768	–	–

C IV resonance lines, without attempting a detailed fit of their profiles, for the same reasons.

3. The wind model and the solution of the radiative transfer equation

3.1. The atmospheric model

Following Catala et al. (1986a), we have assumed a similar wind structure for the stars of our sample, and therefore we can use the same type of model as that of Catala & Kunasz (1987) for AB Aur. We only recall here the basic properties of these models. We assume a steady state non-rotating atmosphere and we consider spherically symmetric winds with a velocity law monotonically increasing outward. The latter is given as linear function of the radial distance *r* from the stellar center. The base of the wind is connected with a classical photosphere model (Kurucz) in radiative and hydrostatic equilibrium at the point where the temperature law in the photosphere reaches a specified minimum $T_{min} < T_{eff}$.

The temperature law in the wind allows to describe a chromospheric temperature rise, and to make its location and its size vary. Four free parameters ($T_0, T_{max}, \Delta_1, \Delta_2$) govern this temperature law, which is expressed by:

$$T(r) = \begin{cases} T_0 + (T_{max} - T_0) exp\left[-4ln2\frac{(r-R_{ch})^2}{\Delta_1^2}\right] \\ \text{if } R_{ph} \leq r \leq R_{ch} \\ T_0 + (T_{max} - T_0) exp\left[-4ln2\frac{(r-R_{ch})^2}{\Delta_2^2}\right] \\ \text{if } R_{ch} < r \end{cases} \quad (1)$$

The maximum temperature is reached in the chromosphere at the point R_{ch} defined by:

$$R_{ch} = R_{ph} + \frac{\Delta_1}{2(ln2)^{1/2}} \left[ln\left(\frac{T_{max} - T_0}{T_{eff} - T_0}\right)\right]^{1/2} \quad (2)$$

R_{ph} being the photospheric radius, while Δ_1 and Δ_2 control respectively the position of the maximum temperature, and the chromospheric extension.

Outside the chromospheric region, the temperature of the wind decreases until it reaches its terminal value T_0; the wind therefore ends up with an isothermal cool region.

Finally, another important parameter of the model is the Doppler random velocity v_D which describes turbulent motions in the wind; this parameter acts as a non thermal broadening component in the intrinsic line profile.

3.2. Solution of the transfer equation for a multi-level atom

For the solution of the transfer equation, we used the method of the equivalent two-level atom (ETLA) in the co-moving frame introduced by Mihalas & Kunasz (1978). A full description of ETLA has been given in Catala & Kunasz (1987). In a first step, ETLA solves the transfer equation together with the equations of statistical equilibrium for three successive ionization stages, in the co-moving frame formulation. Once this step has been performed, calculations in the observers's frame give the emergent flux in the transitions we are interested in, as well as many other physical quantities, like the continuum flux and thereby the value of the Balmer discontinuity, which can directly be compared to observations.

3.3. The atomic models

The atomic model that we have used for hydrogen is made of six bound levels and one continuum, and is identical to that used by Catala & Kunasz (1987); we refer the reader to this paper for more information about the atomic data, and expressions for the transition rates (radiative+collisional).

We have used the same atomic model for carbon as Catala (1988), which includes three levels for C III, two levels for C IV and one continuum level for C V.

For the computation of the Mg II lines, we have introduced five levels for Mg I, seven levels for Mg II, and one continuum level for Mg III. Compared to the model of Catala et al. (1984) in which Mg II is treated as a two level atom, our work represent a real improvement, for both the atomic transitions and the ionization equilibrium are treated in a consistent way. Furthermore, this new model allows us to compute resonance lines to highly excited levels (e.g the 3s-4p λ 1240.1 Å resonance line seen in AB Aur's spectrum), and subordinate lines as well. For Mg II and C IV, the intrinsic line profiles have been assumed Gaussian (in the atomic rest frame), the width of these profiles being calculated from the Doppler random velocity given in the wind model. On the other hand, we have introduced the calculation of the Stark's wings for the $H\alpha$ line, in the observer's frame step.

Table 3. The direction of the arrow indicates the sense of variation of the feature when the parameter is increased - the symbol $\triangle$ indicates that the feature is broadened as the parameter increases

	$H\alpha^{em}$	$H\alpha^{abs}$	$MgII^{em}$	$MgII^{abs}$	CIV^{em}	CIV^{abs}	D_B
Δ_1	—	—	$\searrow$	—	$\nearrow$	$\nearrow$	$\nearrow$
Δ_2	—	—	$\nearrow-\searrow$	—	$\nearrow$	$\nearrow$	$\nearrow$
T_{max}	—	—	$\nearrow$	—	$\nearrow$	$\nearrow$	$\nearrow$
T_0	$\searrow$	—	$\searrow$	$\searrow$	$\nearrow$	$\nearrow$	$\nearrow$
v_D	$\searrow-\triangle$	$\searrow-\triangle$	$\searrow-\triangle$	$\nearrow$	$\searrow-\triangle$	$\searrow-\triangle$	—
$\dot{M}$	$\nearrow-\searrow$	$\nearrow-\searrow$	$\nearrow$	$\nearrow$	—	—	$\searrow$

Auto-ionization and dielectronic recombinations have been neglected, and we have assumed complete redistribution. This latter assumption is justified since partial redistribution effects, that are important for some species in static atmospheres (see Mihalas 1978 or Hubeny 1985 for the case of MgII h and k lines), are likely to be much less important in our case than the effect of Doppler-shift induced by the wind motion. Solar abundances have been assumed. The calculation of the background opacity and emissivity sources is made under the assumption of LTE.

4. Methodology

4.1. Influence of the parameters

The first step of our analysis is to derive a "best fit model" for each one of the stars in our sample, obtained by letting the free parameters vary until a good agreement between the observations of all line profiles and continua and the synthetic ones is reached. Since we are using a large number of lines and continua, formed in various regions of the wind the model derived in this way must represent a realistic description of the average structure of these winds.

However, we are dealing with multi-parameters models so that a "best fit model" is not necessary unique and a detailed analysis of the sensitivity of the synthetic line profiles and continua to the parameters is needed. Such an analysis concerning the Mg II, $H\alpha$ and C IV profiles has been given in Catala et al. (1984), Catala & Kunasz (1987) and Catala (1988) respectively and is extended here to the Balmer discontinuity. All the results are summarized in Table 3.

4.1.1. The mass-loss rate

This parameter influences the density through the continuity equation. The sensitivity of the Balmer jump to the mass loss rate is quite easy to understand. Indeed, as $\dot{M}$ increases, the number of electrons per unit volume increases, thus leading to an excess in the Balmer continuum, which implies a decrease of the Balmer jump.

4.1.2. The velocity law

The velocity law in the wind acts mainly on the lines shapes; its influence on the Balmer discontinuity is rather small. However, we note some characteristic effects. If the velocity everywhere in the wind is increased, the density is decreased (through the equation of continuity) and the contribution of the bound-free emission to the Balmer continuum is weakened, contributing to increase the Balmer jump.

4.1.3. The parameters of the chromosphere

These parameters have been described in Sect. 3. The sensitivity of the Balmer jump to these parameters is quite important; D_B rises when T_{max}, Δ_1 or Δ_2 increase and conversely. Most noticeably, D_B is highly modified by a variation of the location of the maximum of temperature of the chromosphere, determined by parameter Δ_1. If Δ_1 is lowered, the Balmer jump is lowered in turn. The reason of this behaviour is found in the dependance of the radiative recombination rate in both the electron density, n_e, and the electron temperature, T_e, in the region under consideration. Indeed, it can be shown (appendix A) that the radiative recombination rate of hydrogen can be written as: $R_{k\rightarrow i} \propto n_e T_e^{-1/2}$. When the maximum of temperature in the chromosphere is reached in a region of higher density (ie, as Δ_1 is lowered), the radiative recombination rate is brought up, and the bound-free emission in this region shortward of the Balmer jump increases, thus leading to a smaller Balmer discontinuity.

4.1.4. The external temperature

This parameter controls the electron temperature in outer region of the wind and therefore affects the radiative recombination rates (see Sect. 4.1.3).

If this parameter is changed, the size of the Balmer discontinuity changes in the same direction. Indeed, a decrease of T_e implies an increase of the radiative recombination rates which control the flux emitted in the Balmer continuum. This flux produced by the external region is added to the stellar flux, contributing to decrease the Balmer discontinuity.

4.1.5. The temperature minimum

The Balmer jump decreases if the temperature minimum is decreased and conversely. This behaviour is explained by the same mechanism as for the external temperature; nevertheless, hydrogen being predominantly neutral in the region of temperature minimum, the influence of this parameter is quite important.

Table 4. Limits on the parameters.

Parameters	AB Aur	BD+46°3471	HD250550	BD+61°154
Δ_1	[0.14–0.19]	[0.045–1.5]	[0.06–0.11]	[0.082–1.15]
Δ_2	[1.5–2.5]	[1.–2.1]	[1.3–3]	[0.08–2.1]
$T_{max}(K)$	[15000–18000]	[15000–21000]	[17000–22000]	[17000–25000]
T_0 (K)	[3000–5800]	[3000–5100]	[3800–7250]	[3300–6000]
v_D(km/s)	[40–50]	[35–45]	[15–25]	[5–15]
$\dot{M}(10^{-8} M_\odot \cdot \mathrm{yr}^{-1}$	[1.5–2.1]	[7.0–9.1]	[2.75–3.8]	[4.0–6.1]

4.1.6. The Doppler random velocity

As expected, we found no influence of this parameter on the Balmer discontinuity.

In Table 3, we summarize the respective influence of each of the parameters of the model on the lines and continuum features we have modelled.

4.2. Limits on the parameters

Once the "best fit" model is obtained, we can search for upper and lower limits on each one of the parameters, taking into account the available observations and their variability as described in Sect. 2.3, and using the parameter sensitivity analysis presented in Sect. 4.1.

As far as BD+61°154 is concerned, rough limits on T_{max}, Δ_1 and Δ_2 were obtained thanks to the dependence of D_B on these parameters (see Sect. 4.1.3). With the mass loss rate fixed at the value giving the lower (resp. upper) limit of D_B as measured by Garrison (1978), we let T_{max}, Δ_1 and Δ_2 vary until the upper (resp. lower) limit of D_B is obtained (T_0 being fixed at the temperature of a grey atmosphere in radiative equilibrium). Limits on both the maximum temperature and the chromospheric extension are deduced for AB Aur and HD250550 from the known dependence of the C IV profile (Catala 1988) in T_{max} and Δ_2: with temperatures lower than 15000K in AB Aur and 17000K in HD250550, there is not enough C IV to produce absorption lines as deep as those observed, whatever Δ_2. Catala (1988) showed that an emission component appears on the red side of the C IV line with increasing Δ_2, which is never observed; the upper limit on Δ_2 is obtained, with T_{max} fixed to its lower value, as soon as the undetected red emission component induced by the volume emission reaches a level that would make it detectable. For AB Aur, HD250550 and BD+46°3471, limits on Δ_1 are obtained as follows: with T_{max} and Δ_2 and $\dot{M}$ fixed to produce a Balmer discontinuity as weak as possible, we increase Δ_1 until D_B is larger than the upper value of Garrison (1978) and select the corresponding values as the upper limit; we proceed conversely for the lower limit. We have found that the limits on Δ_1 obtained by this method contain those obtained if the profiles of Mg II or C IV were used. If T_{max} is too high, the intensity of the red emission component of C IV is increased because of the enhancement of the line source function. We then used the lower limit on Δ_1 to obtain upper and lower limits on T_{max} and Δ_2 respectively. With this lowest Δ_1, we select the value of Δ_2 that gives the lowest volume emission; the upper limit of T_{max} is the one giving a red emission that can not be lowered by any further decrease of the chromospheric extension. T_{max} and Δ_2 were varied until a clear disagreement with the emission component of the observed profiles of the Mg II line was obtained in the case of BD+46°3471 since no observations of C IV are available. As regards the Doppler velocity, Catala & Kunasz (1987) have shown that it affects both the position and the intensity of the emission component of the $H\alpha$ line. We checked that whithin an interval of $\pm 5 km.s^{-1}$ around the optimal value, we still obain a satisfactory agreement with the observed profiles. After this step, we are left with three parameters: $\dot{M}$, the external temperature T_0 and the velocity law in the region above the chromosphere. The problem to tackle is how to obtain limits on the mass loss rates from the fitting of the $H\alpha$ profile and the Balmer discontinuity. We see from Table 3 that two regimes of $\dot{M}$ exist to fit the observations when only the $H\alpha$ emission is considered, as detailed in Catala & Kunasz (1987). However, the regimes with the highest values for $\dot{M}$ have been discarded as they systematically lead to Balmer excesses larger than observed. At this point, we have to make some simple physical assumptions on T_0, because both the emission component of the $H\alpha$ line and D_B vary in the same way ($n_e T_0^{-1/2}$) with this parameter. It is reasonable to consider that a lower limit on T_0 is given by the temperature of an envelope in grey radiative equilibrium, evaluated at the middle of the zone where the emission of $H\alpha$ forms. If used with the velocity law that gives the highest emission component, this lower value of T_0 provides us with a lower limit on the mass loss rate, the latter being adjusted until a good agreement with the $H\alpha$ emission profile and D_B is obtained. On the other hand, since it is much more difficult to fix an upper limit on T_0, we can not evaluate an upper limit on $\dot{M}$ with the same arguments. Nevertheless, a value for $\dot{M}$ can be found above which the Balmer excess is higher than the observed one; this latter value is the upper limit for the mass loss rate. Thanks to the upper limit for $\dot{M}$, we can deduce an upper limit on T_0, by applying the same operating procedure than before: we choose the velocity law that gives the highest emission component, and with $\dot{M}$ fixed at its upper limit, we let T_0 vary until a good agreement with the $H\alpha$ emission profile and D_B is achieved.

The limits on the mass loss rates presented here also take into account the variations of the lines that we have mentioned in paragraph 2.3.

All the values we found are listed in Table 4 for the four stars under consideration.

5. Detailed comments on individual stars

In the following, we present the detailed results we have obtained when modelling the winds of the four stars presented above.

5.1. AB Aur

Although this star has been fully studied in the past years, we decided to include it in our sample for the following reasons:

1. The first evaluation of the wind structure was made by modelling Mg II as a two level system. We are now able to perform more accurate calculations of the formation of Mg II lines and continua, in the ETLA approach.
2. We have now at our disposal a mean $H\alpha$ profile, averaged over several rotational periods (from the 1996 MUSICOS campaign, Catala et al. 1998). Such an average profile is perfectly suited for our time-independant, spherically symmetric model of the average wind structure of AB Aur. We are also able to compute the Stark wings of this line which constitutes a significant progress compared to the study of Catala & Kunasz (1987), since it is likely to bring new constraints on the wind structure.
3. The high quality data of the C IV resonance doublet spectral region from HST show whithout a doubt that the C IV 1550 Å line has no emission component on its red side, which was controversial on older IUE data. This is a strong observational constraint on the temperature run within the chromosphere.

Moreover, AB Aur is spectroscopically variable and it may be useful to investigate what changes in its wind structure are witnessed by the profile variations; for instance, the emission component of $H\alpha$ has changed by almost 100% between 1987 and 1996. The same kind of dramatic changes occured for the Mg II emission component, which changed from F/F_c=1.9 to F/F_c=2.3; the blue edge of the absorption component indicates terminal velocities of about $V_S = 430 km.s^{-1}$, quite different from that given by the profiles recorded in 1981 ($V_S = 380 km.s^{-1}$). On the spectrum displayed here, the absorption component is almost saturated, contrary to the one presented in Catala et al. (1986a), which implies that the absorption on the line of sight was drastically increased between the two dates of observation (1982 and 1992). Concerning the C IV resonance doublet, we measured a maximum blueward displacement with respect to the rest wavelength of $\Delta V = -260 km.s^{-1}$, about the same as the one shown in Catala & Talavera (1984). We did not try to fit the profile of this line, which would constitute an overinterpretation of the model, but rather used its continuous presence in pure absorption to fix constraints on the maximum of temperature and the size of the chromosphere (see Catala 1988).

We represented the underlying photosphere of this star by a Kurucz model with log(g)=4. and T_{eff}=10000K (Böhm & Catala 1993). Figs. 1–3 present comparisons of computed and observed line profiles for $H\alpha$, Mg II k and C IV 1548 Å lines respectively. The agreement between our calculations and the observations is acceptable for the emission component of the $H\alpha$ line and the Mg II lines. The Stark wings of $H\alpha$ which we have checked are formed in the photosphere underlying the wind are also well reproduced by our model.

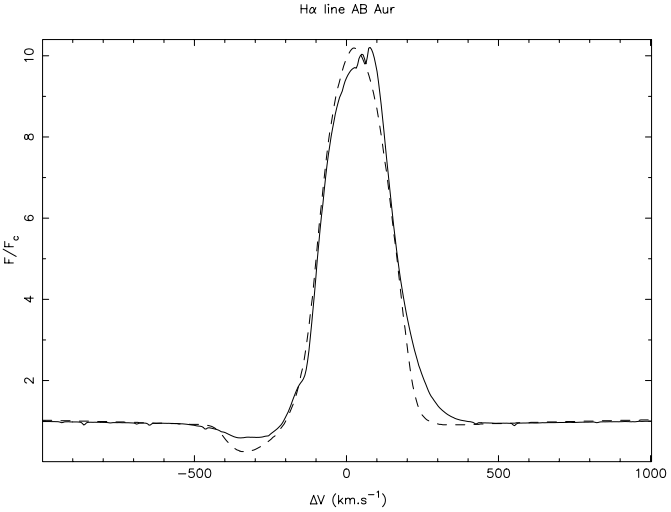

Fig. 1. Observed profile of the $H\alpha$ line (full line), and synthetic $H\alpha$ profile (dashed line) computed for best fit model for AB Aur.

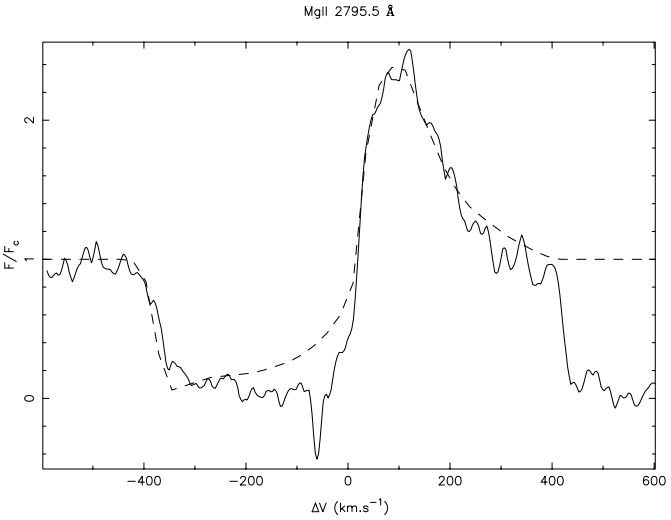

Fig. 2. Observed profile of the MgII k line (full line), and synthetic profile (dashed line) computed for best fit model for AB Aur.

The computed C IV line appears in pure absorption. Since the localization of the continuum is not known in the HST spectrum, we can consider that the agreement between the synthetic and the observed spectrum is satisfactory.

The time variation observed in the line profiles detailed above are likely to be the manifestation of changes occuring in the wind structure. In order to achieve the best agreement with the data set at our disposal, we had to change slightly the values of the parameters of the best fit model found by Catala & Kunasz (1987). It can be seen in Table 5 that in the present model, the chromosphere is located further out in the wind than in their model, with an outer region hotter; on the other hand, the

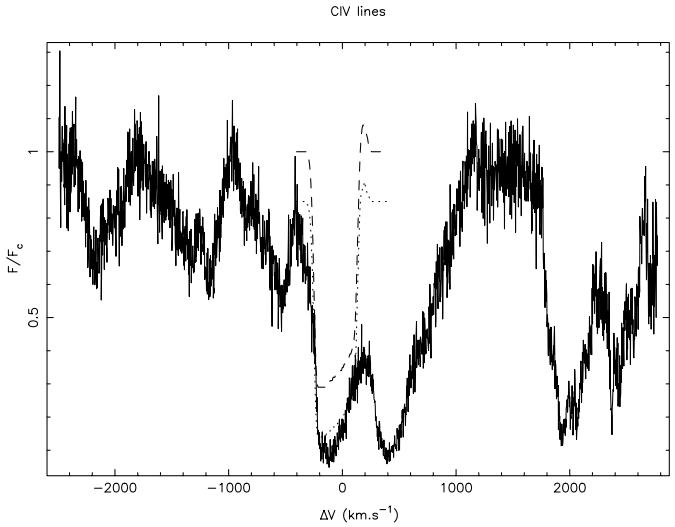

Fig. 3. Observed profile of the C IV line (full line), and synthetic profile (dashed line) computed for best fit model for AB Aur; the dotted line is the "best fit model" scaled for a lower continuum

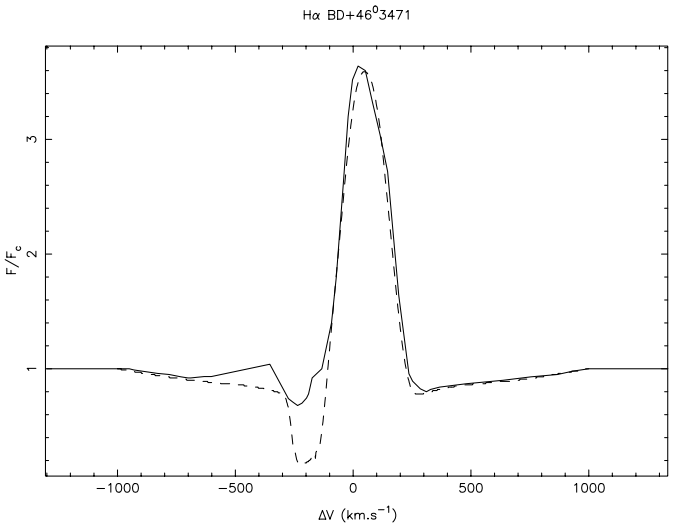

Fig. 4. Observed profile of the $H\alpha$ line (full line), and synthetic $H\alpha$ profile (dashed line) computed for best fit model for BD+46°3471.

Table 5. Parameters deduced from the best fit models.

Parameters	AB Aur	BD+46°3471	HD250550	BD+61°154
Δ_1	0.17	0.08	0.09	0.09
Δ_2	1.5	1.2	1.7	1.0
$T_{max}(K)$	17000	19000	20000	22000
T_0 (K)	4800	4850	4320	3850
v_D(km/s)	45	40	20	10
D_B	1.43	1.06	1.01	0.30
$\dot{M}$ ($M_\odot \cdot \mathrm{yr}^{-1}$)	1.8×10^{-8}	$8.\times10^{-8}$	$3.\times10^{-8}$	4.6×10^{-8}

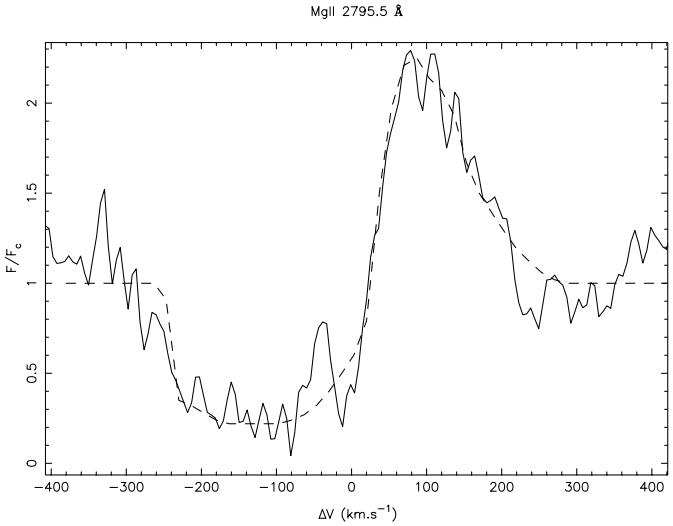

Fig. 5. Observed profile of the MgII k line (full line), and synthetic profile (dashed line) computed for best fit model for BD+46°3471.

maximum temperature as well as the chromospheric extension and the Doppler velocity remain the same which suggests that these quantities may be stable on a period spanning over at least twelve years.

The best fit model presented here has $\dot{M} = 1.8 \times 10^{-8}$ $M_\odot \cdot \mathrm{yr}^{-1}$; this is about half the value found by Nisini et al. (1995) ($\dot{M} = 3.3 \pm 0.01 \times 10^{-8}$ $M_\odot \cdot \mathrm{yr}^{-1}$) (see Sect. 6.2 for a discussion of this difference), but it is of the same order as the value infered by Skinner et al. (1993) from radio measurements. The method described in Sect. 4.2 yields lower and upper limits on $\dot{M}$ presented in Table 4.

Recently, observations with the Hubble space telescope have shown that N V is present in the wind of AB Aur (Bouret et al. 1997). It is not possible to explain these observations with the models we have used in the present study. Bouret et al. (1997) showed that the observed N V lines can be formed in corotating interaction regions (CIRs) bounded by a pair of shocks, where temperatures ranging all the way up to 10^7 K can exist. These CIR can explain at the same time the observed X-ray emission of AB Aur (Zinnecker and Preibisch 1994).

5.2. BD+46°3471

A Kurucz model with log(g)=4.5 and T_{eff}=9500K consistent with the data compiled in the literature (see Table 1) was used to represent the photosphere of this star. Figs. 4 and 5 present the observed profiles of the $H\alpha$ and Mg II line 2795.5 Å lines, over which we plotted our synthetic profiles, for the best fit model. Clearly the agreement is good for the Mg II line and for the emission component of $H\alpha$. The observed small blueshifted emission component cannot be reproduced in the frame work of our models and we comment on it in Sect. 6.1. The shape of the Stark wings is in agreement with the observed one. We also checked that they also match those obtained with the Kurucz model chosen to model the photosphere of this star. As for AB Aur's case, we conclude that these wings are formed whithin the photosphere, where the temperature is decreasing outside.

Despite the time variability of the lines (e.g Catala 1987 reports variations of about 10% rms over five nights for $H\alpha$), our approach allows us to gain information on the global structure of the wind of this star thanks to the emission component which is produced in the major part of the wind. The model that gives the best agreement between the synthetic and the observational profiles gives therefore a rather good representation of at least some characteristics of the wind. The mass loss rate given by this model is $\dot{M} = 8.0 \times 10^{-8}\ M_\odot \cdot \mathrm{yr}^{-1}$; this value is intermediate between the result given by Nisini et al. (1995) i.e, $\dot{M} = 9.6 \pm 0.13\ \times 10^{-8}\ M_\odot \cdot \mathrm{yr}^{-1}$, and the measure by Skinner et al. (1993) ($\dot{M} =\leq 6.5\ \times 10^{-8}\ M_\odot \cdot \mathrm{yr}^{-1}$). As for AB Aur, lower and upper limits of the mass loss rate are listed in Table 4. Whithin these limits, we are able to obtain good fits of the profiles recorded at different dates, particularly for the $H\alpha$ emission component. Finally as for AB Aur, the observed X-ray emission of BD+$46°3471$ (Zinnecker & Preibisch 1994) may perhaps be due to corotating interaction regions.

5.3. HD250550

The Kurucz model for HD250550 has: $T_{eff} = 12000K$ and log(g)=4.5. The Mg II resonance lines of this star were shown to be variable on periods of a few months (Catala et al. 1986a) and the Ca II K line exhibit a short-term variability of a few hours (Catala et al. 1989). The PCygni profiles of the $H\alpha$ line that have been observed in this star in the last years are highly variable and often present complex structures. On the other hand, they exhibit some features that are always observed on all the spectra; particulary, photospheric wings are absent from all these spectra, which is explained by the fact that the wings are probably formed within the wind, in the temperature minimum region where the temperature is slowly varying or is constant. Calculating the Stark wings of $H\alpha$ with ETLA, we have checked that no photospheric wings are seen if the adjacent continuum dethermalizes only in the region of the minimum of temperature or in a region of constant temperature above this minimum. The comparison between the physical spectrum and the synthetic one, (Fig. 6) shows a rather good agreement, at least for the emission component.

Concerning Mg II, Fig. 7 presents the IUE spectrum of the whole doublet because this star behaves quite differently from AB Aur and BD+$46°3471$. The k line emission component is always weaker than the h one, in spite of a higher oscillator strength. The reason may be found in the blend of the k line emission with the absorption component of the h line and the λ2798 Å line. In Fig. 7, it is clear that the λ2791 Å subordinate line of Mg II is strongly blueshifted (95 km.s^{-1}); this phenomenon probably concern the λ2798 Å line as well, which in turn would affect the red side of the k line emission component. Such a blueshift indicates that these subordinate lines are formed whithin the wind rather than in the photosphere, contrary to what seems to happen in AB Aur and BD+$46°3471$.

ETLA being unable to treat line blends, the fitting of the emission component of the k line would be physically meaningless. Thus, we chose to model the h component (2802 Å) which is clearly unaffected by the presence of blends. The agreement between the IUE spectrum and the synthetic profile obtained with the parameters set deduced from $H\alpha$ fitting is quite satisfactory, at least for the emission (see Fig. 7). On the other hand, we did not succeed to fit the absorption troughs (as expected). As regards the C IV line at 1548 Å, we present the result of the computation with the parameters deduced from the study of $H\alpha$ and Mg II h line in Fig. 9; the computed profile is not very different from the observed one considering the uncertainty on the adjacent continuum, and presents no emission on its red side, like in AB Aur's case.

The mass loss rate given by the best fit model is $\dot{M} = 3. \times 10^{-8}\ M_\odot \cdot \mathrm{yr}^{-1}$. This star was observed by Skinner et al. (1993) who found $\dot{M} \leq 5.1 \times 10^{-8} M_\odot \cdot \mathrm{yr}^{-1}$, a result consistent with our calculations.

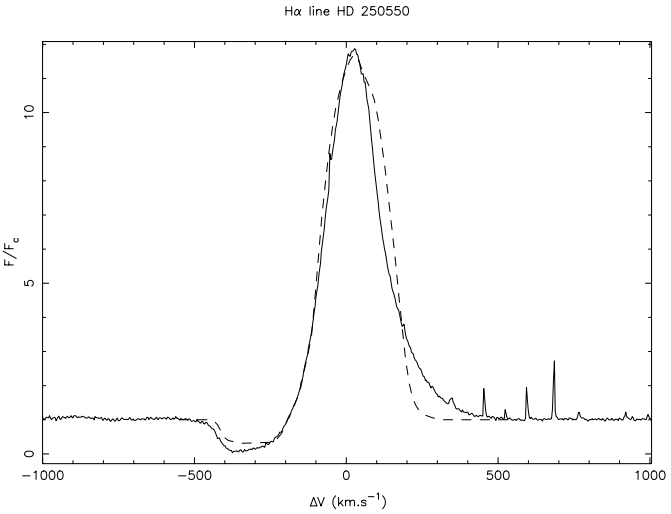

Fig. 6. Observed profile of the $H\alpha$ line (full line), and synthetic $H\alpha$ profile (dashed line) computed for best fit model for HD250550.

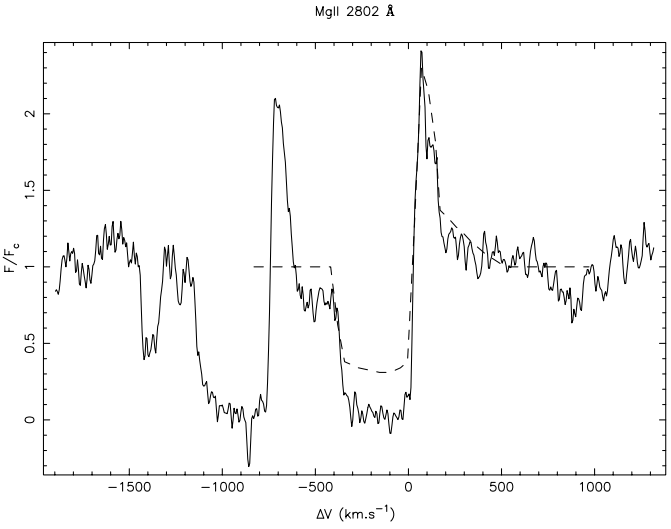

Fig. 7. Observed profile of the MgII h line (full line), and synthetic profile (dashed line) computed for best fit model for HD250550.

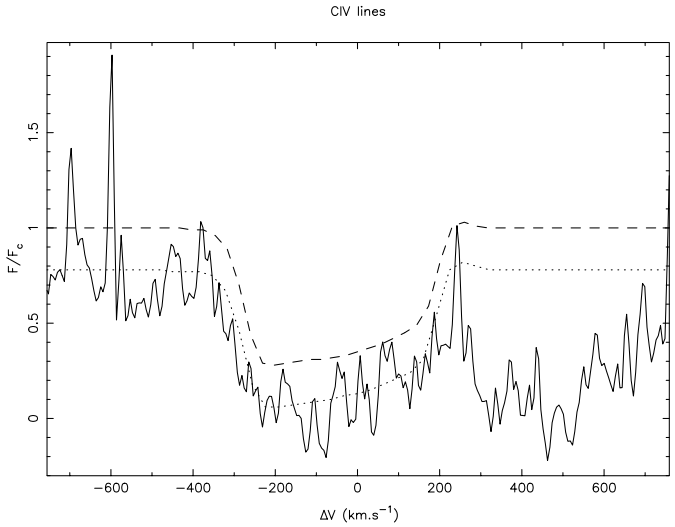

Fig. 8. Observed profile of the C IV line (full line), and synthetic profile (dashed line) computed for best fit model for HD250550; cf Fig. 3 for the dotted line.

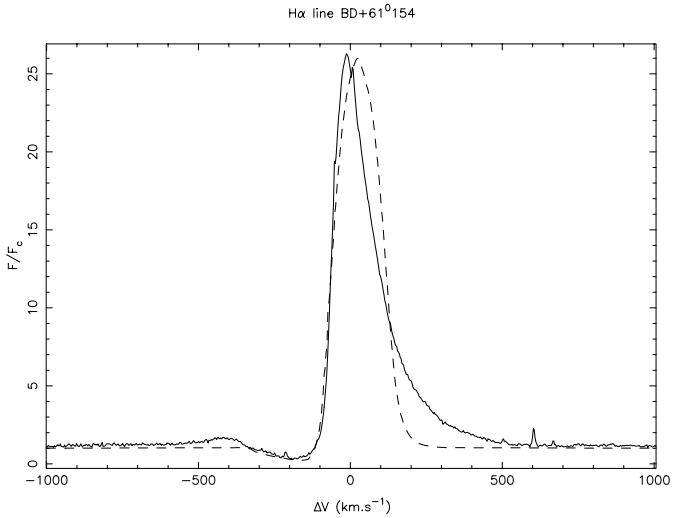

Fig. 9. Observed profile of the $H\alpha$ line (full line), and synthetic $H\alpha$ profile (dashed line) computed for best fit model for BD+61°154.

5.4. BD+61°154

The photosphere of this star is given by a Kurucz's model with T_{eff}=11000K and log(g)=4. In our sample, this star is the only one for which neither IUE nor HST observations are available. Therefore, the parameters we will deduce from the study will be less reliable than for the other stars. The spectral behaviour of this star is quite complex; if compared to spectra presented by Garrison & Anderson (1977) or by Finkenzeller & Mundt (1984), it is clear that dramatic changes occur in the line shape with time. Such changes witness that the physical conditions prevailing in the line formation region are highly variable, the reason of which is still to be adressed.

The profile shown on Fig. 9 is clearly identified as a PCygni profile of type III, in the Beals classification, with a small emission component on the blue side of the line. A closer look at the shape of the blue and red side of this profile shows that this small emission component is symmetric with the broad red wing of the emission component. We checked that when the wings form in the region where the temperature rises, they appear in emission but this process is not efficient enough to bring them to the observed level. Another mechanism was proposed by Mihalas & Conti (1980) to explain such broad red wing extanding very far from the line center and the blue emission component. They suggest that the wind is divided into two distinct regions, one (the deeper) is in corotation with the star, the other is expanding. The superposition of these two motions produce a small emission bump in the blue edge of the line; whether this bump is observed or not depends on the ratio of the rotation velocity to the terminal expansion velocity: if this ratio is greater than one the emission bump is visible otherwise it is blended in the absorption component. The rotation motion also shifts photons from the line center which in turn produce the observed broad line wings. In this framework, the corotation of the envelope is achieved thanks to a global magnetic field, the presence of which is suspected in Herbig Ae/Be stars. However, it would be quite paradoxical that this mechanism would apply for the most slowly rotating star of our sample and would not for stars like HD250550 whose rotation rate is much more important, unless the Alfvén radius is larger in BD+$61^\circ 154$ than in the other stars of the present work. In that case, the angular velocity in the outer parts of the corotating enveloppe could be large enough to explain the line shape. Pogodin (1990) also suggested that PCygni type III profiles could result from the presence of jets with rigid-body rotation, associated with local magnetic region over the surface of the star. He calculated $H\alpha$ profiles for various position of a jet with respect to the observer and concluded that the shape of the line is modified according the phase of the rotation period of the star with its enveloppe. Hence, this mechanism also explains the observed variations of the line shape (from PCygni type III to PCygni type II and conversely). Up to now however, our model does not take such structures into account, which explains why it fails to reproduce such a profile (see Fig. 9). No emission is seen on the blue edge of the synthetic profile, and the red wing of the emission component is far from being broad enough. In the same way, it can not produce an emission component as blueshifted, with respect to the rest wavelength, as the observed one. Such profiles are impossible to obtain with spherically symmetric models, which confirms that the all the discrepancies are probably caused by strong departures from such a geometry in the wind of BD+61°154. This is why our value of $\dot{M}$ is to be considered with precaution; we have found: $\dot{M} = 4.6\times10^{-8}\, M_\odot\cdot\mathrm{yr}^{-1}$; however, variations are allowed (see Table 4), as determined with the method exposed in Sect. 2.4. The value from the best fit model is much lower than that proposed by Nisini et al. (1995), namely $\dot{M} = 1.7 \times 10^{-7}$ $M_\odot \cdot \mathrm{yr}^{-1}$, (obtained from the study of H I infrared lines), but it agrees with that inferred from the radio survey performed by Skinner et al. (1993), namely $\dot{M} \leq 5.9 \times 10^{-8}\, M_\odot \cdot \mathrm{yr}^{-1}$.

6. Discussion

6.1. The absorption components

Because of the extreme sensitivity of the absorption components of PCygni profiles on variations of the physical conditions or geometry of the wind, it is not possible to infer valuable information from their modelling with spherically symmetric and homogeneous models. The results we obtained in the present study can be ordered as follow, if restricted to the $H\alpha$ line: for two stars (AB Aur and BD+$46°$3471) the synthetic absorption trough is deeper than the observed one, while it is the contrary for HD 250550. On the other hand this agreement seems rather satisfactory in the case of BD+$61°$154.

Two stars of our sample, namely BD+$46°$3471 and BD+$61°$154 exhibit a small emission component on the blue side of the line; in one case (BD+$46°$3471) this emission is blended in the Stark wings of $H\alpha$, while in the other case this emission clearly confer to the line a PCygni type III in the Beals classification. Nevertheless, the two others stars have often shown this kind of behaviour in the past (see e.g Catala et al. 1986a). The model presented by Pogodin (1990) (see Sect. 5.4) to explain the episodic appearance of this emission could therefore be applied to all the stars studied presently. In BD+$46°$3471's case, we did not try to obtain a blue-shifted emission component by imposing to the radiation field to be thermalized up to the region of the chromosphere where the temperature is rising, as we did for BD+$61°$154. Indeed, the profile in the first case is clearly not symmetric, the secondary emission being not seen on the red side of the line. This emission being extremely local, it may be formed in a thin region of the wind moving towards us, as suggested by Pogodin's model (1990).

BD+$46°$3471 surely possesses a highly anisotropic wind. Indeed, the vanishing of the absorption component of $H\alpha$, that has been often observed (Garrison & Anderson 1977, Böhm & Catala 1993) implies that our basic assumption of a steady state and spherically symmetric model is unsupported. It is impossible with such a model to avoid an absorption to form. On the other hand, a model like Pogodin's one (1992) succeeds in explaining such a behaviour for the absorption. In this model, the wind is confined at low latitudes, but this confinement is variable. Each time the line of sight intercepts the flow, a PCygni profile is formed. When the opening angle is small enough, the line of sight does not intercept the flow anymore and a single peaked emission is observed. In this framework, we can interpret our situation as follow: at the epoch when the spectra we used were recorded, the opening angle of the wind was large enough for the line of sight to intercept the flow; a PCygni profile is then observed, which is consistent with both the Mg II spectrum and the $H\alpha$ profile. A few years later (see for example Böhm & Catala 1993), the situation is reversed and no PCygni can be observed.

Another interesting fact is that for HD250550, the observed absorption is deeper than the synthetic one for $H\alpha$ as well as for Mg II. In both cases we checked that the observed absorption is saturated. Obviously, an homogeneous model is unable to produce such a deep absorption; indeed, in such a case, a number of photons are scattered towards the observer and then fill in the absorption component, which therefore can not be as deep as the observed one. The observed saturation may be an argument in favour of the interpretation of the cyclical variability of HD250550 in terms of the alternance of streams on the line of sight (on which the absorption is formed) which locally increase the opacity of the medium. As the star rotates, the streams wind up around it and the line of sight may intercept several of them, giving rise to several resonance regions (regions with the same projected velocity); the probability that photons escape is thus lowered. This changes the depth of the absorption component of the PCygni profile. This model had already been proposed by Catala et al. (1991) in order to interpret the periodic variations detected in the short-term variability in the Ca II K line.

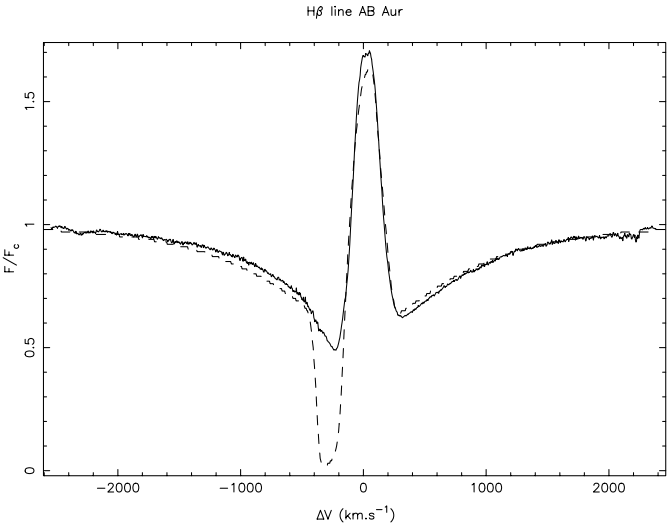

Fig. 10. Observed profile of the $H\beta$ line (full line), and synthetic $H\beta$ profile (dashed line) computed for best fit model for AB Aur.

6.2. Application to other lines

If our models are correct, they must be able to explain the presence and the shape of every lines in the spectra of our program stars. This is in fact the case for the H_β line, whose synthetic profile is compatible with the observed one, at least for the emission component and the Stark wings. Fig. 10 compares our synthetic profile with the observed H_β profile averaged over several days during the MUSICOS 96 campaign. We did not try to fit the other Balmer lines because they are completely dominated by photospheric Stark wings and therefore provide little information on the wind itself.

The Ca II resonance lines are present in all the stars of our sample (Catala et al. 1986a, Finkenzeller & Jankovics 1984). The Ca II K line appears in absorption and asymmetric, extending towards the blue; this suggest that it is formed within the wind. It has been shown in AB Aur's case (Böhm and Catala 1995) that this line is very likely formed in the hottest part of the chromosphere, near the maximum of temperature. On the other hand, the Ca II IR triplet is always seen in emission but blended

with the P13, P15, P16 lines. ETLA being enable to treat lines blends, we did not try to fit these lines. However, we emphasize that the strong similarities that exist between the line profiles of the various stars in our sample, both for the Ca II K line and the Ca II IR triplet strongly supports the idea that the structure of the deepest parts of the wind of the four stars are nearly the same.

6.3. Departure from LTE and mass loss rates

The ionization and excitation conditions in the winds of the stars of our sample are easily obtained with ETLA code. We can therefore deduce the departure from local thermodynamical equilibrium in each point of the wind of a star. In the present section, we will focus on the ionization of hydrogen and its influence on the determination of the mass loss rates. The populations of the levels of our atomic model are strongly different from equilibrium values almost everywhere, except under region of the minimum of temperature, where the continua are formed. The calculations provide us with the transitions rates for all the levels of hydrogen we take into account. We found that the ionization equilibrium is dominated by radiative processes everywhere in the wind for the ground level. For excited levels, ionizations and recombinations are radiatively dominated everywhere but in the chromosphere where collisional processes dominate.

It is thus not surprising that our values of $\dot{M}$ can differ significantly from those derived by Nisini et al. (1995) under the assumption of LTE (up to a factor 4 in the case of BD+$61°154$). The relative agreement between both estimates in the case of HD250550 and BD+$46°3471$ may be simply fortuitous. We stress that the assumption of LTE and the use of lines from a unique chemical element do not allow one to determine reliable values of the mass loss rates. Rather, a number of lines of various elements should be used to get information on the physical conditions all over the wind, leading to a model consitent with all the observational data, as we have done here.

6.4. Radiative losses

The existence of an atmospheric structure of chromosphere+wind seems now well demonstrated for the Herbig Ae/Be stars. Such a structure implies that a large amount of non radiative energy is dissipated in the winds of the Herbig stars. We can estimate it by the calculation of the radiative losses, ie, the amount of energy radiated by the lines and continua that are formed in the wind. We recall here that the radiative losses are defined by:

$$E^-(r) = 4\pi \int_0^\infty \chi_\nu (S_\nu - J_\nu) d\nu \qquad (ergs.cm^{-3}.s^{-1}) \quad (3)$$

It is quite clear from Eq. 3 that smaller radiative losses will be found as the chromosphere will move away from the stellar photosphere: the farther the chromosphere, the lower the density within it, then the lower the energy radiated by the medium.

This equation expresses the total amount of emission minus the total amount of absorption. E^- is then positive when the medium cools by radiation. The sum of the contributions of a large number of radiators and NLTE effects have to be taken into account in the calculation of E^-. In order to calculate $E^-(r)$, we need to solve the radiative transfer equation, that will provide us with the mean radiation intensity as well as with the source function of the transitions we are dealing with. Nevertheless, the lines and continua that have been used up to now do not provide accurate information on the gas physical conditions in the lower part of the chromosphere; we did not introduce this poorly constrained region in our calculations of the radiative losses and computed a lower limit to the energy required to sustain a chromosphere within the wind, E^-, by integrating the radiative losses $E^-(r)$ between the two points r_1 and r_2 where $T = T_{eff}$, r_1 in the inner part and r_2 in the outer part of the chromosphere.

$$E^-_{tot} = \int_{r_1}^{r_2} 4\pi\, r^2 E^-(r) dr \quad (4)$$

For the "best fit" models, the values we have found are listed in Table 6.

For all stars, the dominant contributors to the radiative losses in continua and line are respectively the Balmer continuum and the $H\alpha$ line. It can be seen in Table 6 that the other continua are also efficient radiators, as well as many lines of the Balmer series. Another noteworthy fact is that for BD+$61°154$ and HD250550, the Lyman continuum radiates much more efficiently than for the two other stars of the sample, due to the fact that the Lyman continua of these stars are much less opaque than those of AB Aur and BD+$46°3471$. Finally, it was shown by Catala (1989) for AB Aur, that the other major lines and continua (Magnesium, Carbon) produce negligible contributions to the radiative losses. We have checked that it is the same for the other three stars of our sample.

It is also interesting to notice that, in the case of AB Aur, the Balmer continuum dominates the radiative losses even though the resulting Balmer excess ΔD_B is very small, in agreement with Garrison's (1978) measurements. This result indicates that the Balmer jump measurements, although quite important to constrain the wind and chromosphere parameters, are not sufficient by themselves to estimate the radiative losses.

Uncertainties in the determination of T_{eff} and $\log g$ affect our estimates of the radiative losses, mainly through their effect on the Balmer discontinuity. When T_{eff} or $\log g$ are changed, the contribution of the photosphere to the Balmer jump changes. Hence, the resulting Balmer jump (photosphere + wind) is changed in turn, if the parameters of the wind are kept fixed. The size of the total Balmer discontinuity being mostly determined by the position of the chromosphere, we have to change this parameter to fit the observed D_B. Doing so, we also change our estimates of the radiative losses, which are sensitive to the location and size of the chromosphere within the wind. We investigated these effects, for errors bars on T_{eff} and $\log g$ as given by Hillenbrand et al. (1992) and Garrison (1978) respectively, i.e, $\Delta \log T = 0.05$ and $\Delta \log g = 0.3$.

Table 6. Contributions to the radiative losses

	$E^-_{tot}(ergs.s^{-1})$			
Transition	AB Aur	BD+46°3471	HD250550	BD+61°154
$H\alpha$	1.2 (+32)	1.2 (+33)	1.7 (+32)	5.4 (+32)
$H\beta$	4.3 (+31)	6.0 (+32)	6.6 (+31)	1.8 (+32)
$H\gamma$	4.0 (+31)	5.5 (+32)	4.9 (+31)	1.1 (+32)
$H\delta$	4.6 (+31)	6.2 (+32)	5.2 (+31)	1.0 (+32)
$P\alpha$	1.9 (+31)	1.9 (+32)	2.5 (+31)	7.9 (+31)
$P\beta$	2.1 (+31)	2.3 (+32)	2.3 (+31)	6.9 (+31)
$P\gamma$	2.6 (+31)	3.1 (+32)	2.5 (+31)	6.1 (+31)
$B\alpha$	2.9 (+30)	2.8 (+31)	3.5 (+30)	1.0 (+31)
$B\beta$	5.6 (+30)	6.5 (+31)	5.5 (+30)	1.4 (+31)
$Pf\alpha$	7.7 (+29)	7.3 (+30)	8.7 (+29)	2.4 (+30)
Lyman C.	3.6 (+32)	2.2 (+34)	7.8 (+33)	5.1 (+33)
Balmer C.	1.1 (+34)	5.8 (+34)	3.6 (+34)	3.7 (+34)
Paschen C.	4.9 (+33)	4.1 (+34)	1.8 (+34)	2.0 (+34)
Brackett C.	2.3 (+33)	2.7 (+34)	8.4 (+33)	8.8 (+33)
Pfund C.	1.1 (+33)	1.5 (+34)	3.9 (+33)	4.0 (+33)
Humphrey C.	6.0 (+32)	8.3 (+33)	2.1 (+33)	2.1 (+33)
Total	2.0 (+34)	1.76 (+35)	7.8 (+34)	7.9 (+34)
$E^-_{tot}/L_\star$	0.088	0.044	0.084	0.03
Lower/Upper limits	[1.31–2.4] (+34)	[1.38–5.7](+35)	[0.485–1.16](+35)	[0.61–1.11](+35)

For AB Aur, HD250550 and BD+$61°154$ which all have $T_{eff} \geq 10000K$, we found that for $\log g$ fixed, an increase of T_{eff}, decreases D_B^{phot} so that we have to move the chromosphere away to fit D_B^{obs}. The result is a decrease of the radiative losses compared to those we present here, by an amount of 14%. Concerning the influence of the surface gravity, we found that D_B^{phot} decreases with increasing $\log g$ for these three stars (and conversely). The chromosphere must therefore be further away from the star's surface and the radiative losses can be lowered by an amount of 15% at maximum. The behaviour of BD+$46°3471$, which has $T_{eff} \leq 10000K$, is reversed. Indeed, for $\log g$ fixed, D_B^{phot} varies in the same direction as T_{eff}. Thus, an increase of T_{eff} implies an increase of D_B^{phot}, which in turn requires that the chromosphere must be closer to compensate this effect. This leads to an increase of E^- of the same order of magnitude as for the three other stars. For T_{eff} fixed, $\log g$ affects the radiative losses in the same way as for the three other stars, (direction and amount of the variation).

Using the range of permitted values for all parameters in our models (see Sect. 4.2), we derive lower and upper limits on the contribution to the radiative losses of the chromosphere. We also took into account the uncertainties on $\log g$ and T_{eff} discussed hereabove. Results are listed in Table 6. In terms of stellar luminosity, the radiative losses for the sample of stars under consideration, range from $3\%L_\star$ (for BD+$61°154$) to about $9\%L_\star$ (for AB Aur). These values, although important, are consistent with those found for the T Tauri stars, when measuring the energy flux in some spectral lines and continua (Bouvier 1987, Calvet & Albarran 1984).

Herbig Ae/Be stars being in the radiative phase of their evolution towards the main sequence, convection is unable to be the source of energy that could compensate for these radiative losses. It may be found either in the stellar rotation, through the transformation of rotational energy into turbulent energy through shear instabilities (Lignières et al. 1996) or in the presence of an accretion disk around the stars (Hillenbrand et al. 1992, Corcoran & Ray 1998). The former mechanism provides an energy reservoir lower than the radiative losses by about two or three orders of magnitudes when the effects of the magnetic field are neglected ($E^-_{shear}/E^-_{tot} \propto 10^{-2}$-$10^{-3}$); however, the amount of energy that could be extracted from turbulent subphotospheric layers in presence of magnetic fields is likely to be larger by about two orders of magnitudes (Lignières et al. 1996). This promising approach needs to be completed by its inclusion in a self consistent model of the coupling of the magnetic field production with the turbulent subphotospheric layers and may reconcile the energy production rate with our estimates of the radiative losses.

On the other hand, the model involving an accretion disk seems unlikely for the stars of our sample. Recent millimeter observations of a few Herbig Ae/Be stars, including AB Aur, revealed the presence of elongated structures around the stars (Mannings & Sargent 1997), indicating the existence of circumstellar disks. However, these observations trace the stellar environment at several hundred AU from the star, leaving unexplored the regions forming the lines we are dealing with here. Böhm & Catala (1994) showed that the forbidden [OI] emission lines that arise in their winds are symmetric and unshifted with respect to the rest wavelength, in contrary to what would be expected if a disk were hidding the receding part of the winds. A mechanism assuming that the [O I] forbidden lines form in a thin layer at the surface of the disk (and therefore may not

show asymmetries despite the presence of such disk) has been proposed by Hirth et al. (1994) to reconcile these observations with the presence of an accretion disk. However, this suggestion was recently contradicted by Böhm & Hirth (1997) on the basis of longslit observations, which showed that at least in AB Aur's case, the possibility that the [O I] lines are formed in a disk-atmosphere can be ruled out. For the other stars, the situation is not so clear, even though Böhm & Hirth (1997) found neither significant offset of the emission centroid nor any extension of the line emitting region. If disk-atmospheres are present, they cannot be extended enough to account for the observed fluxes in these lines, as discussed in Böhm (1993) and Böhm & Hirth (1997). In addition, using the accretion rates derived by Hillenbrand et al. (1992), we have checked that the energy released by accretion ($\dot{E}_{acc} = 1/2\dot{M}_{acc}V_{kep}^2$, where V_{kep} is the keplerian rotation velocity as estimated from the width of the [O I] lines) is always lower by a factor of two (in the best case) than the radiative losses we found. Besides, Bo̎hm & Catala (1993) showed that for AB Aur, the accretion rate must be lower than $2.5\,10^{-7} M_\odot \cdot \mathrm{yr}^{-1}$ (i.e at least 6 times lower than that derived by Hillenbrand et al. 1992) to be compatible with the observed absence of optical veiling. Future quantitative calculations of [O I] lines formation should teach us more about the presence or absence of circumstellar disks around these stars. At the present time, the problem of the source of energy responsible for the activity of the Herbig Ae/Be stars is still open.

7. Conclusion

The existence of an expanding extended chromosphere, surrounded by a cool wind is now confirmed for Herbig Ae/Be stars belonging to the PCygni subclass. Semi-empirical models similar to the one developped for AB Aur's wind by Catala et al. (1984), succeed in reproducing as many different lines as $H\alpha$, the Mg II h & k lines or the C IV resonance lines at 1550 Å, as well as the Balmer jump, for three additional stars, and provide us with an accurate description of the structures of their winds.

This semi-empirical modelling allows us to constrain severely the temperature, size and location of the chromosphere, and to derive reliable values of the mass loss rates and radiative losses. The mass loss rates derived in this way are much more reliable than those from previous studies (Nisini et al. 1995, Garrison 1978), based on much more limited observational constraints. The radiative losses in the chromospheres of these stars represent several percent of their bolometric luminosities.

The origin of the large amounts of non-radiative energy that must be deposited in these chromospheres to maintain them is still unknown. Models involving massive accretion disks may be invoked, although their presence around the Herbig stars in our sample is very controversial. Such disks carry sufficient amounts of gravitational energy if their accretion rates exceed $10^{-7}\,M_\odot \cdot \mathrm{yr}^{-1}$. Moreover, radiatively driven winds from accretion disks, such as modelled by Proga et al. (1998) and Drew et al. (1998), may constitute a solution to the so far unexplained winds of the Herbig Ae/Be stars. However, an efficient heating mechanism to explain the chromospheres of these stars in this context has still to be identified.

Alternatively, the ultimate origin of this non-radiative energy may be stellar rotation, transformed into turbulent motions in the star's interior because of the violent rotational braking that the wind exerts on the star's surface (Lignières et al. 1996). In this model, the chromospheric heating is magnetic, which is made plausible by the recent detection of a magnetic field in another Herbig Ae star (Donati et al. 1997).

The hypothetical magnetic field may also be responsible for azimuthal and latitudinal structuration of the winds of the Herbig stars in our sample. This structuration is not taken into account in our modelling, which is spherically symmetric and stationary, but could be responsible for (i) the time variability of line profiles observed in these stars, and (ii) the remaining discrepancies between observed line absorption components and our calculated profiles.

A natural follow-up of this work will therefore be an extension of our modelling to non-spherical geometries, including flattened and azimuthally structured stellar winds.

Acknowledgements. We thank the MUSICOS collaboration for making data available to us prior of publication.

Appendix A

By definition, the radiative photoionization and recombination rates between the i-*th* level of a given ion and the *k* continuum state write respectively:

$$R_{i\to k} = 4\pi \int_{\nu_0}^{\infty} \frac{\alpha(\nu)}{h\nu} J_\nu d\nu$$

$$R_{k\to i} = 4\pi \left(\frac{n_i}{n_k}\right)^* \int_{\nu_0}^{\infty} \frac{\alpha(\nu)}{h\nu} \left(\frac{2h\nu^3}{c^2} + J_\nu\right) \times exp\left(-\frac{h\nu}{kT_e}\right) d\nu$$

ν_0 being the photo-ionization threshold of the level under consideration, while $\alpha(\nu)$ and J_ν are the photo-ionization cross-section and the mean radiation field respectively. T_e is the local electron temperature and $\left(\frac{n_i}{n_k}\right)^*$ is the ratio of the population of the i-*th* level of neutral hydrogen over the one of singly ionized hydrogen respectively, evaluated at thermal equilibrium. So as to calculate $R_{k\to i}$, we will make some approximation on J_ν.

It is well known that for a given ion excitation level, one can define a "dethermalizing layer" for the ionizing radiation field, i.e, a layer where this radiation field begins to depart from the local Planck function. Provided that the opacity of the medium at the wavelength of the ionizing radiation field varies regularly over the wind, we see that the aforementioned dethermalizing layer separates a zone where the radiation field is optically thick and a zone where it is optically thin. In the former regions J_ν is given by the local Planck function, while in the latter we can write:

$$J_\nu \sim W(r) B_\nu(T_r)$$

W(r) being a dilution factor and B_ν being the Planck function evaluated at the "radiation temperature", i.e, the electron temperature at the dethermalizing layer. For W(r), noting R_l for the radius of the dethermalizing layer, we have:

$$W(r) = \frac{1}{2}\{1 - [1 - (R_l/r)^2]^{1/2}\}$$

We can now make use of those approximations in the calculation of $R_{k\to i}$.

In a first time, we will address the problem of the Balmer discontinuity; in such a case, one has $J_\nu \ll 2h\nu^3/c^2$ and we can therefore write that:

$$R_{k\to i} \sim 4\pi \left(\frac{n_i}{n_k}\right)^* \int_{\nu_0}^{\infty} \frac{\alpha(\nu_0)}{h\nu} \left(\frac{\nu_0}{\nu}\right)^3 \left(\frac{2h\nu^3}{c^2}\right) exp\left(-\frac{h\nu}{kT_e}\right) d\nu$$

where we have made use of the following form of the photo-ionization cross-section: $\alpha(\nu) = \alpha(\nu_0)(\frac{\nu_0}{\nu})^3$.

It is then straightforward to see that:

$$R_{k\to i} \sim \frac{8\pi}{c^2}\alpha(\nu_0)\nu_0^3 \left(\frac{n_i}{n_k}\right)^* E_1\left(\frac{h\nu_0}{kT_e}\right)$$

If now, we replace $\left(\frac{n_i}{n_k}\right)^*$ by its literal expression (namely the well-known Saha equation) for the i-*th* level of an hydrogen atom and making use of $E_1(x) \sim x^{-1}e^{-x}$ for $x \gg 1$, we get:

$$R_{k\to i} \sim A.n_e T_e^{-1/2}$$

where

$$A = \frac{8\pi}{c^2}\alpha(\nu_0)\nu_0^3 \left(\frac{h^2}{2\pi mk}\right)^{3/2} \frac{g_i}{2}$$

Hence, we see that increasing the mass loss rates or moving the chromosphere closer to the stellar surface will enhance the recombination rate, thus leading to decrease the Balmer discontinuity.

References

Appenzeller I., Jankovics I., Krauter J., 1983, A&AS 53, 293
Appenzeller I., Jankovics I., Östreicher R., 1984, A&A 141, 108
Baudrand J., Böhm T., 1992 A&A 259, 711
Bertout C., Basri G., Bouvier J., 1988, ApJ 330, 350
Berrilli F., Corciulo G., Ingrosso G., et al., 1992, ApJ 398, 254
Beskrovnaya N.G., Pogodin M.A., Tarasov A.E., Sherbakov A.G., 1991, Pis'ma Astron. Zh. 17, 825 (Soviet Ast. Lett. 17, 349)
Beskrovnaya N.G., Pogodin M.A., Nadjenov I.D., Romanyuk I.I, 1995, A&A 298, 585
Böhm T. 1993 Thèse de Doctorat, Université Paris 7
Böhm T., Catala C., 1993 A&AS 101, 629
Böhm T., Catala C., 1994 A&A 290, 167
Böhm T., Catala C., et al. (25 authors), 1996, A&AS 120, 431
Böhm T., Hirth G.A., 1997, A&A 324, 177
Bouret J.-C., Catala C., Simon T., 1997, A&A 328, 606
Bouvier J., 1987, PhD thesis, Université Paris 7
Calvet N., Albarran J., 1984, Rev. Mex. Astron. Astrof. 9, 35
Catala C., 1988, A&A 193, 222
Catala C., 1989, 4 th Colloque IAP, in honor of J.C. Pecker, Modelling the Stellar Environment: How and Why, Paris, eds: Ph. Delache, S. Laloe, C. Magnan, J. Tran Thanh Van, p. 207
Catala C., Kunasz, P.B., Praderie F., 1984, A&A 134, 402
Catala C., Praderie F., Kunasz P.B., 1984, A&A 154, 103
Catala C., Talavera A., 1984, A&A 140, 421
Catala C., Czarny J., Felenbok P., Praderie F., 1986a, A&A 154, 103
Catala C., Felenbok P., Czarny J., Talavera A., Boesgaard A.M., 1986b, ApJ 308, 791
Catala C., Praderie F., Felenbok P., 1986, A&A 182, 115
Catala C., Kunasz P.B., 1987, A&A 174, 158
Catala C., Felenbok P., Czarny J., Talavera A., Thé P.S., 1991, A&A 244, 166
Catala C., Böhm T., Donati J.-F., Semel M., 1993b, A&A 278, 187
Catala C., Böhm T., Donati J.-F., et al., 1994, Solar Phys. 155, 185
Cohen M., Kuhi L.V., 1979, ApJs 41,743
Corcoran M., Ray T., 1997, A&A 321, 189
Corcoran M., Ray T., 1998, A&A 331, 147
Donati J.F., Semel M., Carter B.D., Rees D.E., Cameron A.C., 1997, MNRAS 291, 658
Drew J., Proga D., Stone J.M., 1998, MNRAS L6-L10
Eggen O.J., 1995, AJ 110, 1749
Finkenzeller U., Jankovics I., 1984, A&AS 57, 285
Finkenzeller U., Mundt R., 1984, A&AS 55, 109
Garrison L.M., 1978, ApJ 224, 535
Garrison L.M., Anderson C.M., 1977, ApJ 218, 438
Ghandour L., Strom S., Edwards S., Hillenbrand L., 1994, In: Thé P.S, Pérez M.R., van den Heuvel E.P.J (eds.) Nature and evolutionary status of Herbig Ae/Be stars, Astron. Soc.Pac.Conf.Ser. 62, p.223
Hamman F., Persson S.E., 1992a, ApJs 82, 285
Hartmann L., Kenyon S.J., Calvet N., 1993, ApJ 407, 219
Hillenbrand L., Strom S.E., Vrba F., Keene J., 1992, ApJ 397, 613
Hirth G.A., Mundt R., Solf J., 1994, A&A 285, 929
Hubeny I., 1985, In: J.E. Beckmann J.E., Crivellari L., Reidel, Dordrecht (eds.) Progress in Spectral Line Formation Theory
Kenyon S.J., Hartmann L., 1987, ApJ 323, 714
Koresko Ch.D., Beckwith S.V.W., Ghez A.M., Matthews K., Neugebauer G., 1991, AJ 102, 2073
Kurucz R.L., 1979 ApJS 40, 1
Lignières F., Catala C., Mangeney A., 1996, A&A 314, 465
Mannings V., Sargent A., 1997, ApJ 490, 792
Mihalas D., In: Stellar Atmospheres, 2nd edition
Mihalas D., Conti P.S., 1980, ApJ 235, 515
Mihalas D., Kunasz P., 1978, ApJ 219, 635
Nisini B., Milillo A., Saraceno P., Vitali F., 1995, A&A 302, 169
Palla F., Stahler S.W., 1990, ApJ 360, L47
Palla F., Stahler S.W., 1991, ApJ 375, 288
Palla F., Stahler S.W., 1922, ApJ 392, 667
Palla F., Stahler S.W., 1993, ApJ 418, 414
Pezzuto S., Strafella F., Lorenzetti D., 1997, ApJ 485, 290
Pogodin M.A., 1990, Astrofisika 32, 371
Pogodin M.A., 1992, Pisma Astron. Zh. 18, 1066
Pogodin M.A., 1994, A&A 282, 141
Praderie F., Simon T., Catala C., Boesgaard A.M., 1986, ApJ 303, 311
Proga D., Drew J., Stone J.M., 1998, MNRAS 295, 595
Shevchenko V.S., 1991, Pis'ma Astron. Zh. 17, 347 (Soviet Ast. Lett. 17, 146)
Shevchenko V.S., Vitrichenko E.A., 1994, In: Thé P.S, Pérez M.R., van den Heuvel E.P.J (eds.) Nature and evolutionary status of Herbig Ae/Be stars, Astron. Soc.Pac.Conf.Ser. 62, p.55
Skinner S.L., Brown A., Stewart R.T., 1993, ApJs 87, 217
Strom S.E., Strom K.M., Yost J., Carrasco L., Grasdalen G.L., 1972, ApJ 173, 353
Tout C.A., Pringle J.E., 1995, MNRAS 272, 528
Vigneron C., Mangeney A., Catala C., Schatzman E., 1990, Solar Phys. 128, 287
Yoshida S., Kogure J., Nakano M., 1991, Publ. Astron. Soc. Japan 43, 363
Zinnecker H., Preibisch Th., 1994 A&A 292, 152